REPORT DOCUMENTATION PAGE

Form Approved
OMB No. 0704-0188

1. REPORT DATE *(DD-MM-YYYY)*	2. REPORT TYPE	3. DATES COVERED *(From - To)*
	Technical Paper	

4. TITLE AND SUBTITLE

Please see attached

5a. CONTRACT NUMBER

5b. GRANT NUMBER

5c. PROGRAM ELEMENT NUMBER

6. AUTHOR(S)

5d. PROJECT NUMBER
2308

5e. TASK NUMBER
M19B

5f. WORK UNIT NUMBER
346058

7. PERFORMING ORGANIZATION NAME(S) AND ADDRESS(ES)

ERC

8. PERFORMING ORGANIZATION REPORT

9. SPONSORING / MONITORING AGENCY NAME(S) AND ADDRESS(ES)

Air Force Research Laboratory (AFMC)
AFRL/PRS
5 Pollux Drive
Edwards AFB CA 93524-7048

10. SPONSOR/MONITOR'S ACRONYM(S)

11. SPONSOR/MONITOR'S NUMBER(S)
Please see attached

12. DISTRIBUTION / AVAILABILITY STATEMENT

Approved for public release; distribution unlimited.

13. SUPPLEMENTARY NOTES

14. ABSTRACT

15. SUBJECT TERMS

16. SECURITY CLASSIFICATION OF:			17. LIMITATION OF ABSTRACT	18. NUMBER OF PAGES	19a. NAME OF RESPONSIBLE PERSON
a. REPORT	b. ABSTRACT	c. THIS PAGE			Leilani Richardson
Unclassified	Unclassified	Unclassified	A		19b. TELEPHONE NUMBER *(include area code)* (661) 275-5015

FILE 2308 #198

MEMORANDUM FOR PRS (In-House Publication)

FROM: PROI (STINFO) 16 Mar 2001

SUBJECT: Authorization for Release of Technical Information, Control Number: **AFRL-PR-ED-TP-2001-060**
Vaghjiani, Ghanshyam L. (ERC), "Gas Phase Reaction Kinetics of O-atoms With (CH3)2NNH2, CH3NHNH2 and N2H4, and Branching Ratios of the OH Product"

Journal of Physical Chemistry **(Statement A)**
(Deadline N/A)

Gas Phase Reaction Kinetics of O-atoms With $(CH_3)_2NNH_2$, CH_3NHNH_2 and N_2H_4, and Branching Ratios of the OH Product

Ghanshyam L. Vaghjiani

ERC, Inc.
Air Force Research Laboratory
AFRL/PRSA
10 E Saturn Blvd
Edwards AFB, CA 93524
Tel: 661 275 5657
Fax: 661 275 6245
Email: ghanshyam.vaghjiani@edwards.af.mil

ABSTRACT

The gas phase reaction kinetics of O-atoms with the two alkylated di-amine rocket fuels $(CH_3)_2NNH_2$ and CH_3NHNH_2 was studied in a discharge flow-tube apparatus under pseudo-first-order conditions in [O-atom]. Direct vuv cw-resonance fluorescence monitoring of the [O-atom] temporal profiles in a known excess of the [di-amine] yielded the following absolute second-order O-atom rate coefficient expressions; $k_1 = (1.94 \pm 0.34) \times 10\text{-}11\ e^{(25 \pm 25)/T}$ and $k_2 = (2.29 \pm 0.40) \times 10\text{-}11\ e^{(-145 \pm 40)/T}$ cm^3 molec-1 s-1, respectively, for reactions with $(CH_3)_2NNH_2$ and CH_3NHNH_2 in the temperature range 232-644 K and in He pressure of 2.0 torr. The total yields of OH in the reactions were measured to be (0.12 ± 0.09) and (0.14 ± 0.10) at 298 K and in 2.0 torr He pressure. Close to ~ 53% and ~ 59% of the OH produced was estimated to be vibrationally excited. A pulsed-photolysis reactor was used to extend our measurements on the O-atom reaction kinetics with the unsubstituted rocket fuel, N_2H_4, that we

had previously studied in the flow-tube apparatus. At 298 K, both the rate coefficient, k_3 = (0.59 ± 0.12) x 10^{-11} cm^3 $molec^{-1}$ s^{-1} and the total OH yield = (0.35 ± 0.14) did not show any discernable dependence on He or N_2 buffer gas pressures of up to 404 torr. The magnitude of the weak temperature dependence and the lack of pressure effects in the O + N_2H_4 reaction rate coefficient suggests that simple direct metathesis of H-atom may not be important compared to initial addition of the O-atom to the di-amine, followed by rapid dissociation of the intermediate into a variety of products.

INTRODUCTION

Hydrazine (N_2H_4), methylhydrazine (CH_3NHNH_2) and unsymmetrical dimethylhydrazine ($(CH_3)_2NNH_2$) form an important class of di-amine based rocket fuels.[1] They are typically oxidized in nitrogen tetroxide (N_2O_4) combusters to generate the desired thrust. For example, a blend of 50:50 N_2H_4 and $(CH_3)_2NNH_2$ is deployed in the Titan launch vehicles and CH_3NHNH_2 is used in the various Space Shuttle thrusters that make up the Orbital Maneuver System (OMS) and the Reaction Control System (RCS). Their use as monopropellants, especially that of N_2H_4, is also very common in small attitude and trajectory control systems of many satellites. Rocket exhaust effluents, which can include raw fuel fragments, are known not only to reduce the lifetime or the performance of the onboard instrumentation due to surface contamination,[2] but also to degrade the ambient atmospheric optical environment due to chemiluminescent interactions both in the near and far-fields of the expanding plume. Emissions ranging from the ir to the vuv are possible that primarily arise due

to on going combustion reactions in the near-field (core-radiation)[3] and due to effluent-atmosphere collisions in the far-field (plume-radiation).[4-8] The most recent ground-based[9] and in-flight[4,10] observations of the uv-visible emissions from the Space Shuttle's thrusters have reported intense 336-nm NH(A→X) and 630-nm O(^{1}D→^{3}P), and strong 558-nm O(^{1}S→^{1}D) features in the plume-radiation. Analysis and modeling of these features as a function of ram-angle and altitude indicate that the mechanism for O(^{1}S)/O(^{1}D) production is via collisional excitation of atmospheric O(^{3}P) by the exhaust effluents, H_2O and/or N_2, and for NH(A) production via the O(^{3}P) + CH_2NH reaction. The CH_2NH fragment is believed to come from the thermal decomposition of the escaping fuel, CH_3NHNH_2. Clear explanations of the source(s) for many other weaker emission features (OH(A→X), NO(A→X), CN(B→X) and CO(a→X) etc.) in Space Shuttle plume-radiation have not yet been proposed. This must wait until we have a detailed understanding of the processes that control the temporal and spatial evolution of the initial exhaust effluents and their subsequent products. The three main processes that determine the fate of the di-amine fuel fragments within the thermospheric plume are degradation by pyrolysis, oxidation by O-atoms and heterogeneous loss to spacecraft surfaces. It is therefore desirable to accurately determine the product distributions and the reactivity trends in O-atom reactions with di-amines not only for carrying out reliable plume-radiance calculations but also for properly simulating the combustion of these fuels in N_2O_4.

There is only one previous report[11] on the room temperature (296 K) values for the O-atom rate coefficients; $k_1 = (2.3 \pm 0.34) \times 10^{-11}$ and $k_2 = (1.6 \pm 0.34) \times 10^{-11}$ cm^3 molec^{-1} s^{-1}, respectively, for reaction with $(CH_3)_2NNH_2$ and CH_3NHNH_2. In the same study $k_3 = (0.99 \pm$

0.12) x 10-11 cm^3 molec-1 s-1 for the O + N_2H_4 reaction was also reported. Two other room temperature values for k_3 = (0.30 ± 0.15) x 10-11 and = 1.82 x 10-11 cm^3 molec-1 s-1 can also be found in the literature.[12,13] All these values differ significantly from our previous value of (0.61 ± 0.11) x 10-11 cm^3 molec-1 s-1 measured in a flow-tube apparatus.[14] Furthermore, we measured a negative temperature dependence for k_3 = (7.35 ± 2.16) x 10-13 x exp[(640 ± 60)/T], in the temperature range 252-423 K and in 2.0 torr He pressure, whereas a positive dependence of 1.4 x 10-10 x exp[-604/T] cm^3 molec-1 s-1 in the temperature range 243-463 K and in 1-10 torr of Ar pressure had been claimed in Ref. 13. Accurate product yield measurements in the above three reactions are also scarce. For O + N_2H_4 reaction, an OH yield of (0.15 ± 0.05) at 298 K and in 2.0 torr of He pressure was previously reported by us.[14] This low yield is consistent with Foner and Hudson's[15] mass spectrometric observations of N_2H_3 product intensity being ~ 25 times smaller than that of the N_2H_2 product in their crossed molecular beam investigations of the O + N_2H_4 interaction. Similarly, in the O + $(CH_3)_2NNH_2$ interaction, they identified the $(CH3)_2NNH$ product but no mass signal corresponding to the $(CH3)_2NN$ product was seen. And finally in the O + CH_3NHNH_2 interaction, the products CH_3NNH (not CH_3NHN) and CH_3NHNH or CH_3NNH_2 were identified. No actual yields for the carbonaceous species were reported. However, from these product studies they concluded that the predominant simultaneous abstraction of two H-atoms in the O + $N_2H_4 \rightarrow N_2H_2 + H_2O$ reaction must be occurring by the removal of one hydrogen from each of the nitrogens. It follows that this mode of O-atom attack is probably negligible in the O + $(CH_3)_2NNH_2$ reaction but is competitive with the single-H-atom removal, O + $CH_3NHNH_2 \rightarrow OH + CN_2H_5$, in the case of methylhydrazine's reaction. Similarly, in another mass spectrometric study by Gerhing

and co-workers,[13] a relatively large signal for the primary H_2O product compared to OH was also observed in the O + N_2H_4 system.

In this study the temperature dependencies of k_1 and k_2, in the range 232-644 K and in 2.0 torr He pressure, are reported for the first time, and the effect of pressure on k_3(298 K) investigated for He or N_2 buffer gas pressures of up to 404 torr. We have also measured the OH product yields at 298 K in these reactions and used this information to gain some further insight into the nature of the reaction mechanism in the O + di-amine system.

EXPERIMENTAL TECHNIQUE

Previously, we have described the details of the fast flow-tube apparatus and the pulsed-photoylsis reactor.[14,16] Here, we only give the details of reagent preparations, and how the reaction kinetics data were collected and analyzed.

The di-amine plus O-atom reactions were studied under pseudo-first-order conditions in O-atom concentration ([O-atom] << [di-amine]). The gas phase [di-amine] concentration in the experiments was determined by uv photometric techniques, and accurate measurements of the system's pressure, temperature and carrier gas flow rates using previously calibrated capacitance manometers, thermocouples and electronic mass-flow meters. The uv-absorption cross sections, σ213.9-nm of 220.5 x 10-20, 248.9 x 10-20 and 399.9 x 10-20 cm^2 molec-1, respectively for N_2H_4, CH_3NHNH_2 and $(CH_3)_2NNH_2$ were used.[16,17] The Teflon/Pyrex flow-lines were

previously conditioned with the di-amine so that its in-situ decomposition in the reactors was negligible. For the fast flow-tube apparatus, the O-atoms were generated either in a fixed side-arm or in a sliding-injector microwave discharge port. A 1% O_2 in He mixture was discharged to produce the O-atoms. The inside walls of the port were coated with a 30% solution of H_3PO_4 acid to minimize O-atom loss before being injected into a known amount of the di-amine being carried by He with a total linear bulk-flow velocity, v. The di-amine entered the main reaction zone of the flow-tube from the sliding-injector when the O-atoms were produced upstream in a side-arm, and from the side-arm when the O-atoms were made in the sliding-injector. The flow-tube was operated under plug-flow conditions[18] at a nominal He pressure of 2.0 torr and in the temperature range 232-644 K. A halocarbon coated Pyrex flow-tube with an outer Pyrex jacket that contained a thermostated cooling/heating fluid was used for temperatures below 373 K, and a resistively heated quartz flow-tube (previously cleaned in H_3PO_4 solution) was used for higher temperature work. Data below 232 K was not obtained as the loss rate of O-atoms to the walls in the presence of the di-amine was so high that the signal-to-noise ratio of the O-atom resonance fluorescence fell below the detection limit of ~ 5 x 10^8 molec cm^{-3} (signal-to-noise ratio = 1, 1-sec integration time). The flow-tube had to be warmed to 232 K or above in order to recover the O-atom signal to its original level. Similarly, data above 644 K was not collected as the tendency for charring inside the flow-tube due to alkylated di-amine decomposition was observed to increase greatly for $T \geq 650$ K. At each [di-amine], the kinetics of the O-atom plus di-amine reaction was followed by recording the steady-state O-atom cw-resonance fluorescence signal strength as a function of the reaction distance, z between the point of reagent mixing at the injector tip and the fixed detection zone downstream of the flow-tube. The O-atoms were probed using a cw-microwave atomic resonance lamp to excite the ($3^3S_1 \leftarrow 2^3P_J$) transitions in atomic

oxygen. The 130.2-130.6-nm resonance fluorescence ensuing from the detection zone was detected orthogonally to the lamp using a vacuum-monochromator/PMT assembly. The signals were analyzed using photon-counting/multichannel scaling techniques and recorded at a microcomputer for later analysis.[14] The OH product profiles were recorded with sufficient H_2O added to the flow-tube mixture that it preferentially quenched any OH(v" > 0) formed to its ground (v" = 0) state before any significant reactive loss took place.[19] The OH was probed using a tunable pulsed-laser operating at ~ 282.15 nm to excite the Q_12 line of the OH transition ($A^2\Sigma^+$, v' = 1 ← $X^2\Pi$, v" = 0). The resulting laser-induced fluorescence due to the transitions ($A^2\Sigma^+$, v' = 1 → $X^2\Pi$, v" = 1, bandhead at 312.16 nm) and ($A^2\Sigma^+$, v' = 0 → $X^2\Pi$, v" = 0, bandhead at 306.36 nm), ensuing from the detection zone was detected orthogonally to the probe laser beam by a second bandpass-filter/PMT assembly. These signals were analyzed using gated charge-integration/signal averaging techniques and recorded at another microcomputer.[14,20] The detection limit for OH was estimated to be ~ 1 x 10^9 molec cm^{-3} (signal-to-noise ratio = 1, per 1000-pulse-integrations).

A pulsed-photolysis reactor operating under slow-flow conditions was employed to extend the k_3(298 K) rate coefficient measurements for the O + N_2H_4 reaction in He or N_2 buffer gas pressures of up to 404 torr. 248-nm laser photolysis (1–5 mJ/cm^2/pulse) of ~ 1.0 x 10^{13} molec cm^{-3} of ozone ($O_3 + h\nu \rightarrow O(^1D) + O_2$, followed by $O(^1D) + N_2 \rightarrow O(^3P) + N_2^*$) was employed to directly follow the kinetics of $O(^3P)$ in excess N_2H_4 by recording the cw time-resolved resonance fluorescence O-atom signal immediately after the photolysis pulse. The O-atom rate coefficient data in N_2 was also obtained indirectly by monitoring OH production in the

reaction. Here, 193-nm photolysis of N_2O was used to produce the $O(^3P)$ and excess CO_2 was used as the OH(v" > 0) product quencher.[19] The kinetics was followed by determining the [OH] time profile immediately after the photolysis by recording the relative OH-fluorescence signal strength as a function of the delay time between the photolysis and probe laser pulses. The slow gas flow rate of the reactor and the laser repetition rate were chosen so as to replenish the reaction mixture in the detection zone after every photolytic pulse.

The absolute OH product yields in these reactions were determined by measuring the relative detection sensitivity for O-atoms and OH radicals in our apparatuses using suitable photolytes for which the values of OH and/or $O(^3P)$ quantum yields are accurately known. This is described in detail in the next section.

Materials

He (> 99.9997%) from U. S. Bureau of Mines, N_2 (99.9995%) from Spectra Gases, N_2O (99.99%) from Matheson Gas Products and CO_2 (99.99%) from Scott Specialty Gases were used as received. Hydrocarbon-free N_2H_4 (Viking Grade) from Edwards AFB, $(CH_3)_2NNH_2$ (> 99.3%) and CH_3NHNH_2 (> 99.5%) from Olin Chemicals were subjected to several freeze-thaw purification cycles at a grease-less vacuum line, and the purified distillates dried over BaO or CaH_2. O_2 (99.991%) from Big Three Industry was used as supplied to make up a 1% in He discharge mixture. O_3 was generated by flowing the O_2 through a commercial ozonator and collected in a trap over silica gel at 195 K. Excess O_2 entrained in the gel was pumped off at 77

K. A 2% O_3 in He calibration mixture was prepared in a darkened 12-*l* flask. The water was distilled in the laboratory.

RESULTS

Direct k_1, k_2 and k_3 Determinations

Since the [di-amine] always is in a great excess over the [O-atom] in the flow-tube, it can be shown that the pseudo-first-order decay coefficient, k'_i, for O-atoms is given by; $\ln\{OS/OS_O\} = -k'_i.t.$ Where OS is the net (background-subtracted) steady-state O-atom cw-resonance fluorescence signal strength recorded at the detection zone for a reaction time of $t = z/v$. The flow-tube reaction distance, z, is defined to be the length between the tip of the sliding-injector where the O-atoms enter and the O-atom resonance fluorescence detection axis. v is the bulk linear flow velocity of the He carrier gas. OS_O is the net signal strength that would be observed for $z = 0$ and corresponds to the initial concentration, $[O\text{-atom}]_o$ available at the detection zone. $k'_i = k'_W + k_i[\text{di-amine}]$, where k'_W is the first-order loss rate term for O-atoms to the walls, and k_i the absolute second-order O-atom reaction rate coefficient with the di-amine (i = 1 or 2 for $(CH_3)_2NNH_2$ and CH_3NHNH_2, respectively). Values of k'_i in the range 100-600 s^{-1} were extracted from non-linear-least-squares fits to the data points of the observed exponential decays of the O-atom signal. In the absence of the di-amine, k'_W was typically found to be ~ 10-20 s^{-1} at 298 K. (For O-atoms entering upstream via the fixed side-arm port, there is additional loss of

O-atoms, which increases as the reaction length is decreased due to increasing amount of exposure to the sliding-injector walls. In this case it can be shown that $k'_i = - k'_{w,in} + k_i[\text{di-amine}]$, where $k'_{w,in}$ is the first-order decay coefficient for O-atom loss at the injector walls. This lost rate term, $k'_{w,in}$ was typically found to be ~ 5 s^{-1} at 298 K, see Figure 1, open circles). The values of k'_i were plotted as a function of [di-amine] to extract the corresponding k_i values by fitting the data to a linear-least-squares routine, see Figure 2. Figure 3 shows the temperature dependencies of k_1 and k_2 in the range 232-664 K and in 2.0 torr He pressure.

In the $O_3/N_2/N_2H_4$ pulsed-photolysis experiments, the O-atom signal immediately after the initiating laser pulse was also observed to decay exponentially, with the decay coefficient, k'_3 given by; $k'_d + k_3[N_2H_4]$. Here, k'_d represents the sum of first-order loss rate terms of O-atoms due to diffusion out of the detection volume, and reaction with O_3 and background impurities. k'_d was typically measured to be in the range 25-50 s^{-1} and k'_3 in the range 500-3000 s^{-1}. The 298 K values of k_3 determined from second-order plots were; (0.56 ± 0.08) x 10^{-11}, (0.55 ± 0.08) x 10^{-11} and (0.60 ± 0.09) x 10^{-11} cm^3 $molec^{-1}$ s^{-1} in 21.6 torr He, 208.9 torr He and 205.4 torr N_2 pressure, respectively. All indicated errors in this work are 1-σ, precision plus estimated systematic.

OH Product Yield Measurements

The exothermicity of the O + di-amine reaction can produce OH with internal vibrational excitations up to the limit of available reaction enthalpy.[14] In order to be able to measure accurately the total OH yield in the reaction by just probing the (v" = 0) level, and be able to extract a rate coefficient value for the OH + di-amine reaction, it was necessary to record the OH profile in the presence of a suitable quencher that allowed rapid relaxation of OH(v" > 0) to the ground state compared to its reactive and/or diffusional loss.

It can be shown that the [OH] profile in the O + di-amine flow-tube reaction can be represented by;

$$[OH] = \{(A-B)/(k'_i-k'_{i,OH})\}*\{\exp(-k'_{i,OH}.t)-\exp(-k'_i.t)\}+\{B/(k'_v-k'_{i,OH})\}*\{\exp(-k'_{i,OH}.t)-\exp(-k'_v.t)\} \quad (I)$$

Where $k'_{i,OH} = k_{i,OH}[\text{di-amine}] + k'_{w,OH}$ represents the pseudo-first-order loss of OH in the system, with $k_{i,OH}$ as the absolute second-order rate coefficient for OH reaction with the di-amine and $k'_{w,OH}$ as the first-order rate term for loss to the flow-tube walls. $k'_v = k_{i,OH^v}[\text{di-amine}] + k_{OH^v}[H_2O] + k'_{r,OH^v} + k'_{w,OH^v}$ is the effective first-order rate term for decay of vibrationally excited hydroxyl radicals in the system (depicted as OH^v for all v" levels), with k_{i,OH^v}, k_{OH^v}, k'_{r,OH^v} and k'_{w,OH^v}, respectively, as the second-order rate coefficient for reaction with the di-amine, the second-order rate coefficient for quenching with water, the radiative decay coefficient and the first-order rate term for loss to the walls. The term coefficients are given by; $A = f_{i,OH}k_i[O]_o[\text{di-amine}]$ and $B = ((k_{OH^v}[H_2O] +$

$k'_{r,OH^V})f_{i,OH^V}k_i[O]_o[\text{di-amine}])/(k'_i-k'_v)$, where $f_{i,OH}$ and f_{i,OH^V} are the branching fractions for production of OH in (v" = 0) and all excited states, respectively. For our flow-tube conditions during yield measurements of 4.0×10^{15} of H_2O quencher and $(0.4\text{-}1.1) \times 10^{13}$ molec cm^{-3} of di-amine concentrations, the second term of Equation (I) is negligible, and the expression reduces to: $[OH] = ((f_{i,OHtot} \cdot k_i[\text{di-amine}][O]_o)/(k'_i-k'_{i,OH}))*\{\exp(-k'_{i,OH}.t)-\exp(-k'_i.t)\}$, where $f_{i,OHtot}$ represents the total OH branching fraction in the reaction. The recorded [OH] profiles can thus be fitted, without significant errors, to a 3-variable bi-exponential expression of the form; $m_1*\{\exp(-m_2.t)-\exp(-m_3.t)\}$ to extract values for k'_i from m_3, $k'_{i,OH}$ from m_2, and the total OH yield from m_1.

Figure 4(a) shows a typical [OH] profile recorded in the O + CH_3NHNH_2 flow-tube reaction. Figure 5(a) shows values for k'_2 (solid triangles) extracted as a function of [CH_3NHNH_2] employed in the experiment as well as those measured by directly monitoring the O-atom decay in the same experiment (open triangles). Figure 5(b) shows the corresponding plot for $k'_{2,OH}$ values. The slopes in these plots give absolute second-order rate coefficient values of $k_2(298\ K) = (1.38 \pm 0.34) \times 10^{-11}$ (OH-monitoring) and $(1.43 \pm 0.25) \times 10^{-11}$ (O-atom monitoring), and $k_{2,OH}(298\ K) = (5.6 \pm 1.7) \times 10^{-11}$ cm^3 $molec^{-1}$ s^{-1} in 2.0 torr He. The corresponding $(CH_3)_2NNH_2$ flow-tube values in 2.0 torr He were $k_1(298\ K) = (2.01 \pm 0.49) \times 10^{-11}$ and $(2.10 \pm 0.37) \times 10^{-11}$, and $k_{1,OH}(298\ K) = (6.7 \pm 2.0) \times 10^{-11}$ cm^3 $molec^{-1}$ s^{-1}.

The photolysis reactor was used to extend the OH yield measurements to higher buffer gas pressures in the O + N_2H_4 reaction. N_2O (5.0×10^{15} molec cm^{-3}) was photodissociated at

193 nm (1.5 mJ/cm^2/pulse) in the presence of N_2 to generate the $O(^3P)$, and the OH profile recorded with sufficient CO_2 (8.1 x 10^{16} molec cm^{-3}) also present to preferentially relax the vibrationally excited OH to its ground state before significant reactive loss occurred. Figure 4(b) shows a typical OH plot obtained, and the line is a fit to the data points for a kinetic expression analogous to Equation (I). At each of the 21.2, 185.8 and 404.0 torr of N_2 pressures studied, the absolute second-order rate coefficient values of $k_3(298\ K) = (0.63 \pm 0.16) \times 10^{-11}$, $(0.60 \pm 0.15) \times 10^{-11}$ and $(0.62 \pm 0.16) \times 10^{-11}$, and $k_{3,OH}(298\ K) = (3.9 \pm 1.2) \times 10^{-11}$, $(3.8 \pm 1.1) \times 10^{-11}$ and $(3.2 \pm 1.0) \times 10^{-11}$ cm^3 molec^{-1} s^{-1}, respectively, were deduced from the OH profiles. Direct O-atom monitoring (to deduce k_3) in these experiments was not performed since the N_2O caused a severe loss in the resonance fluorescence signal due to its huge absorption cross section at ~ 130 nm.[21]

Extraction of the absolute branching fraction for OH production in the O + di-amine reactions from fitted values of m_1 (using m_2 and m_3) requires instrument calibration using a suitable photolyte. In the flow-tube work, it can be shown that;

$$m_1(m_3-m_2)(R^O/R^{OH})/^OS_o = (f_{i,OH} + \sim f_{i,OH}{}^v)k_i[\text{di-amine}] \qquad \text{(II)}$$

Where ^OS_o is the O-atom signal at z = 0 determined directly from the [O-atom] decay recorded in the same experiment as the [OH] profile. (R^O/R^{OH}) is the relative response factor for O-atom and OH detection at the two detector assemblies. This is determined in a back-to-back calibration experiment by photodissociating a small amount of O_3 (2.0 x 10^{13} molec cm^{-3}) at

193 nm (1.5 mJ/cm^2/pulse) in the detection volume of the flow-tube with the same amount of H_2O (4.0 x 10^{15} molec cm^{-3}) and He (2.0 torr) present as that employed in the kinetic runs. This ensured that the detection sensitivity for O-atoms and OH radicals remained unchanged in the back-to-back runs. The exponential [OH] and [O^3P] decays are simultaneously recorded in the calibration run, keeping the O-atom microwave lamp output and OH-probe laser energy the same as that used in the kinetic run. Care is taken to ensure that the 193-nm photolysis laser beam completely encapsulates the counter propagating light beam from the microwave lamp inside the detection volume. The signals are extrapolated to time zero to determine the value for the ratio of the initial OH and O-atom signals, $(^{OH}S_{o,cal}/^{O}S_{o,cal}) = (R^{OH}/R^{O})([OH]_{o,cal}/[O]_{o,cal})$. The ratio, $([OH]_{o,cal}/[O]_{o,cal})$ for the initial OH and O-atom production is directly calculable from the known OH yield in H_2O photolysis,[22,23] $O(^1D)$ and $O(^3P)$ yields in O_3 photolysis,[24] and product yields in $O(^1D) + H_2O$ and $O(^1D) + O_3$ reactions.[25] Since a large excess of $[H_2O]$ relative to [di-amine] is employed, the weak [di-amine] dependence of the f_{i,OH^v} term is ignored in the analysis. Also, it can be shown that under these conditions, ~ 98 % of the OH(v" > 0) will be quenched to the ground state. Therefore, the value of $(f_{i,OH} + \sim f_{i,OH^v})$ will underestimate the true total OH yield by only ~ 2% or so. Figure 5(c) shows a plot of $m_1(m_3-m_2)(R^O/R^{OH})/^{O}S_o$ as a function of $[CH_3NHNH_2]$, whose slope gives a value for $(f_{2,OH} + \sim f_{2,OH^v})k_2(298\ K) = (0.20 \pm 0.10)$ x 10-11 cm^3 molec^{-1} s^{-1} as the phenomenological rate coefficient for the channels that lead to OH formation. Similar analysis for O + $(CH_3)_2NNH_2$ system gave $(f_{1,OH} + \sim f_{1,OH^v})k_1(298\ K) =$ (0.24 ± 0.12) x 10-11 cm^3 molec^{-1} s^{-1}. An estimate for f_{i,OH^v} in the flow-tube reactions was

made in a different kind of back-to-back experiment. Here, the Q1(1) line of the OH(0←0) transition was probed and the resulting fluorescence in the (0→0) band observed in the presence (4.0×10^{15} molec cm^{-3}) and absence of added water at a fixed (~ 2 ms) reaction time. The signal ratio, OHS_{water}/OHS is, to a good approximation, directly proportional to $(f_{i,OH} + {\sim}f_{i,OH^V})/f_{i,OH}$, provided OHS_{water} is corrected for the drop in the OH fluorescence quantum yield when water is present in the detection volume. Such analyses at 298 K yielded values of ~ 53% and ~ 59% for f_{1,OH^V} and f_{2,OH^V}, respectively.

Also using the above OH excitation/detection scheme, the phenomenological OH yield in the O + N_2H_4 reaction was determined by comparing the laser induced fluorescence signal observed in the 193-nm photolysis of $N_2O/N_2/CO_2/N_2H_4$ mixture to that seen in $N_2O/N_2/CO_2/H_2O$. It can be shown that;

$$m_1(m_3-m_2)(OHf_{water}/OHf)(D/C)/OHS_{o,water} = (f_{3,OH} + {\sim}f_{3,OH^V})k_3[N_2H_4] \qquad \text{(III)}$$

Where m_i (i = 1-3), as before, are the best values to a bi-exponential fit of the [OH] time profile in $N_2O/N_2/CO_2/N_2H_4$ photolysis, $OHS_{o,water}$ is the time-zero OH signal in $N_2O/N_2/CO_2/H_2O$ photolysis, and OHf_{water} and OHf represent the OH-fluorescence quantum yield terms in $N_2O/N_2/CO_2/H_2O$ and $N_2O/N_2/CO_2/N_2H_4$ photolysis, respectively. D = $([N_2O]\sigma_{N_2O}Y^{OH} + [H_2O]\sigma_{H_2O})$ and C = $([N_2O]\sigma_{N_2O}Y^{O} + [CO_2]\sigma_{CO_2})$, with Y^{OH} = $(1.92[H_2O]k_{H_2O})/([CO_2]k_{CO_2} + [N_2]k_{N_2} + [N_2O]k_{N_2O} + [H_2O]k_{H_2O})$ and Y^{O} = $([CO_2]k_{CO_2} + [N_2]k_{N_2} + 0.04[N_2O]k_{N_2O})/([CO_2]k_{CO_2} + [N_2]k_{N_2} + [N_2O]k_{N_2O})$. The

various $k_{species}$ are the second-order rate coefficients for O^1D reactions with the species[25] and the $\sigma_{species}$, the absorption cross sections at 193 nm.[22,25,26] The first term in C represents the amount of O^1D from N_2O photolysis that converts to O^3P and the second term the amount of O^3P from direct photolysis of CO_2. Similarly in D, the first term represents the amount of O^1D that converts to OH upon replacing N_2H_4 with excess H_2O and the second term the amount of OH from direct photolysis of H_2O. Calculations of these terms, for our experimental conditions, showed that the contribution to O^3P from CO_2 photolysis[26,27] was small compared to that from N_2O[25], and contribution to OH from H_2O photolysis[22,23] comparable to that from O^1D conversion.[25] The ratio, $(OHf_{water}/OHf) = (k'_{rad} + [CO_2]q_{CO_2} + [N_2]q_{N_2} + [N_2O]q_{N_2O})/(k'_{rad} + [CO_2]q_{CO_2} + [N_2]q_{N_2} + [N_2O]q_{N_2O} + [H_2O]q_{H_2O})$ is calculable from the known OH(A, v' = 0) quenching rate coefficients, $q_{species}$[28] and the radiative decay rate, k'_{rad},[29] and the measured species concentrations. This ratio was maintained close to unity (it ranged from 0.989 to 0.927) by using just sufficient amount of water (8.0×10^{15} molec cm^{-3}) in the calibration run to convert a small amount (1.5-12.0%) of the O^1D to OH. The small contribution from N_2H_4 in OHf and YO is ignored in the above analysis. The slopes in the plots of Equation (III) yielded the values; $(f_{3,OH} + {\sim}f_{3,OH^v})k_3(298\ K) = (0.20 \pm 0.06) \times 10^{-11}$, $(0.24 \pm 0.07) \times 10^{-11}$, and $(0.21 \pm 0.06) \times 10^{-11}$ cm^3 molec^{-1} s^{-1}, respectively for N_2 pressures of 21.2, 185.8 and 404.0 torr.

DISCUSSION

Reaction Kinetics and OH Yield Measurements. The reactions of O-atoms with the di-amines are fast, and show weak temperature dependencies. The Arrhenius fits to the data points of Figure 3 give the following expressions; $k_1 = (1.94 \pm 0.34) \times 10\text{-}11\ e^{(25 \pm 25)/T}$ and $k_2 = (2.29 \pm 0.40) \times 10\text{-}11\ e^{(-145 \pm 40)/T}$ cm^3 $molec^{-1}$ s^{-1}, respectively, for reactions with $(CH_3)_2NNH_2$ and CH_3NHNH_2 in the temperature range 232-644 K and in He pressure of 2.0 torr. Variation in the initial O-atom concentration, $[O]_o$ from 1 x 10^{11} to 7 x 10^{11} molec cm^{-3} in the flow-tube had no systematic effect on the k_i(298 K) values, showing that the influence of any secondary O-atom reactions on the rate coefficient determinations is negligible. Previously[14] we had shown that O-atoms produced by N_2 microwave discharge followed by N-titration with NO gave the same values for k_3 as did the O_2 discharge source. Therefore $O_2(^1\Delta)$ from the O_2-discharge is expected to have a negligible effect, if any, on our k_1 and k_2 determinations. The k_3(298 K) values obtained in the present photolysis reactor are consistent with our earlier values from the flow-tube apparatus. Variation in the 248-nm photolysis fluence (in the range 1-5 mJ/cm^2/pulse) had no detectable effect on the measured value of k'_3. Thus interference from N_2H_4 photolysis products was also negligible. The O_3 photolyte was added just upstream of the photolysis zone to prevent its excessive loss due to reaction with N_2H_4. During the mixture's residence time of ~ 0.25 seconds in the reactor, less than 1.7% O_3 loss was estimated to occur for the case when the highest $[N_2H_4]$ was employed. The products ($OH + O_2 + N_2H_3$)[30] of this reaction are also expected to cause a negligible interference to our rate measurements. No attempt was made to measure k_1 and k_2 by photolyzing O_3 in $(CH_3)_2NNH_2$

or CH_3NHNH_2 (in the presence of N_2) since these mixtures are expected to be more than 10 times or so less stable than the O_3/N_2H_4 mixture.[30]

Also, no discernable pressure effect on k_3(298 K) was observed for up to 404 torr of He or N_2. Our average value for k_3(298 K) in this work is (0.59 ± 0.12) x 10^{-11} cm^3 $molec^{-1}$ s^{-1}. The present flow-tube k_1(296 K) and k_2(296 K) values are in excellent agreement, within ~ 10% and ~ 14%, respectively, to those of Lang's determined in a photolysis reactor,[11] though their k_3(296 K) value is ~ 68% higher than ours. Assuming that the [di-amine] can be measured accurately in these two studies (to within ± ~ 6% in our work), the presence of reactive impurities in Lang's sample of N_2H_4 may be a possible cause for the higher measured rate coefficient. The present values of $k_{1,OH}$(298 K) = (6.7 ± 2.0) x 10^{-11}, and $k_{2,OH}$(298 K) = (5.6 ± 1.7) x 10^{-11} in 2.0 torr He and the average value of $k_{3,OH}$(298 K) = (3.6 ± 1.2) x 10^{-11} cm^3 $molec^{-1}$ s^{-1} in up to 404 torr He or N_2 pressure are entirely consistent with our direct flow-tube measurements of (6.0 ± 1.1) x 10^{-11}, (6.1 ± 1.1) x 10^{-11} and (3.7 ± 0.7) x 10^{-11} cm^3 $molec^{-1}$ s^{-1}, respectively.[31]

The phenomenological branching fraction, $B_{i,OH}$, for total OH yield in the reactions can be calculated from the ratio of the measured slope(s) of Equation (II) (or III) and the corresponding fitted value of k_i. These were; $B_{1,OH}$ = (0.12 ± 0.09) and $B_{2,OH}$ = (0.14 ± 0.10) at 298 K and in 2.0 torr He, and $B_{3,OH}$ = (0.32 ± 0.13), (0.40 ± 0.15) and (0.34 ± 0.13), respectively, in 21.2, 185.8 and 404 torr N_2, and 298 K. Our previous $B_{3,OH}$ value determined in the flow-tube work was (0.15 ± 0.05) at 298 K and in 2.0 torr He. In both the flow-tube and

photolysis work we consistently measure a low phenomenological yield for OH in the $O + N_2H_4$ reaction, though the agreement in the absolute values is not within the combined error limits of the two measurements. The value from the photolysis work is probably more reliable than that from the flow-tube work since much better fits in the OH profiles were possible in this method as data points could be recorded at very short reaction times (~ 100 μs) and also at very long reaction times where the signal approached to the background level. In the latter flow-tube method, the shortest reaction time used was restricted to ~ 1 ms to ensure mixing of the reagents downstream of the flow-tube had attained a steady-state condition, and the longest time possible was ~ 12 ms due to the physical limit of our flow-tube length. Also from Equation (III) it can be seen that the extracted $(f_{3,OH} + {\sim}f_{3,OH^v})k_3$ value relies on only knowing the $[N_2O]$ and $[H_2O]$ accurately in the calibration run. These we measured directly using electronic mass flow-meters and 184.9-nm photometry, respectively. Both compounds undergo unit dissociation at 193 nm, via a single photolysis channel, to give $(O^1D + N_2)$ and (H + OH) as the products.[23,25] However, in the flow-tube work (Equation (II)), not only must the $[H_2O]$ and $[O_3]$ (measured by 253.7-nm photometry) be known correctly, an accurate value is also needed for the ratio of the quantum yield, $\Phi(O^3P):\Phi(O^1D)$ in the dissociation of ozone, which is known to be a multi-channel process at 193 nm. Previously, we have directly determined $\Phi(O^1D)$ and $\Phi(O^3P)$ to be (0.46 ± 0.29) and (0.57 ± 0.14), respectively.[24] Therefore, $\Phi(O^3P)/\Phi(O^1D)$ may be in the range 1.54-0.93. Thus, re-analysis of our earlier work shows that $(f_{3,OH} + {\sim}f_{3,OH^v})k_3$ can range from 1.16×10^{-12} to 0.67×10^{-12} cm^3 $molec^{-1}$ s^{-1}. If we include this variability with our flow-tube measurement uncertainties, the nominal value of (0.15 ± 0.11) makes the previous phenomenological OH yield in reasonable agreement with the present work. The average value

of the two methods is (0.30 ± 0.17). This low phenomenological OH yield (in the N_2H_4 + O-atom reaction is qualitatively in agreement with Foner and Hudson's[15] measurements of low signals for the hydrazyl radical (the co-product of OH) relative to that for the di-imide, N_2H_2, and Gehring and co-worker's[13] low signals for the OH product relative to that for H_2O (the co-product of N_2H_2).

The O-atom reactions with $(CH_3)_2NNH_2$, CH_3NHNH_2 and N_2H_4 show significant internal vibrational excitation in the OH product. Our relative measurements provide estimates of ~ 53%, ~ 59%, and ~50%,[14] respectively. Production of OH(v" = 1) in the alkylated di-amine + O-atom reactions (in the absence of added H_2O quencher) was also independently verified in this work by observations of weak LIF signals where the hydroxyl radical was directly excited in the (1←1) band, and the resultant (1→0) and (1→1) band emissions monitored at a monochromator/PMT assembly. No discernable OH LIF signals were seen for (2←2) laser excitation. Thus most of the vibrationally excited OH is thought to be produced in (v" = 1) state with approximately < 5% of the OH in (v" > 1) levels.

The low OH yields determined in all three O + di-amine reactions mean that removal of a single H-atom is a minor process at 298 K. Hence direct H-abstraction by the O-atom from N-H bonds, and when available from C-H bonds plays a relatively minor role in the overall reaction mechanism. Removal of hydrogen atom(s) could also well occur in an addition-elimination process. The observed negative temperature dependencies of k_i, for T < 500 K, and the lack of pressure effect on k_3 or $B_{3,OH}$ in up to 404 torr of N_2 pressure would be consistent with the formation of an adduct that rapidly dissociates, in principle, through several different product

channels. Formation of a cyclic reaction adduct with the O-atom bridged between two H-atoms could either eliminate H_2O (plus the azo co-fragment) in simultaneous breaking of two N--HOH-N bonds, or OH (plus the hydrazyl co-fragment) in a sequential breaking of the N-H--O bond followed by the O-H--N bond. Bridging may take place either across 2 H-atoms at the same nitrogen or between 2 H-atoms, each one of which is situated at the 2 different nitrogens. Foner and Hudson[15] concluded that this different-N type of bridging is favored in O + CH_3NHNH_2 reaction since the mass spectrometric appearance signal of m/e = 44 ion for (cis) CH_3NNH (and not the di-radical, CH_3NHN) could be identified with a stable di-imide product,[32] while no m/e = 58 ion signal for the $(CH_3)_2NN$ product was seen at all in the case of O + $(CH_3)_2NNH_2$ reaction. It could well be that CH_3NHN and $(CH_3)_2NN$ are also formed via the same-N kind of bridging, but their rapid rearrangement/dissociation prevented them from being detected in their system. For example, highly excited azomethane would be expected to form from $(CH_3)_2NN$ rearrangement in the O + $(CH_3)_2NNH_2$ reaction. The reaction exothermicity of ~ 102 kcal mol^{-1} in this channel would be sufficient to dissociate the azomethane into $2CH_3 + N_2$. Previously, it is been shown that photo-excited azomethane (at 193 nm) does indeed fragment, after an efficient trans → cis or trans → gauche isomerization, by the rupture of two C-N bonds via a concerted mechamism.[33] It remains an open question whether chemically-activated azomethane in its various isomeric forms if produced in the O + $(CH_3)_2NNH_2$ reaction also dissociates similarly. Thus, direct mass spectrometric detection of the primary product, H_2O (or the CH_3 and N_2 fragments of the co-product) would have been more desirable in Foner and Hudson's work to show whether this mode of O-atom attack on $(CH_3)_2NNH_2$ was important or not. Our low OH yield in O + $(CH_3)_2NNH_2$ reaction would

either support this or the possibility that yet another type of addition adduct is involved in these reactions. The observed increase in the room temperature reaction rate coefficient along the series: N_2H_4, CH_3NHNH_2, $(CH_3)_2NNH_2$, with rate ratios, 1.0:2.3:3.5, shows that increased methylation is facilitating the formation of such adduct(s). This would be consistent if the O-atom, acting as an electrophile, attaches preferentially to the substituted N-atom, where the relative electron charge density would be expected to increase with increased methylation along the homologous series. Evidence for such a process may be found in the related amine homologous series; CH_3NH_2, $C_2H_5NH_2$, $(CH_3)_2NH$, $(CH_3)_3N$, where the room temperature O-atom rate coefficient was observed to increase from left to right, and was independent of the argon buffer gas pressure of 13 to 52 torr employed,[34] showing here also that H-abstraction from N-H is probably not a predominant reaction path. The observed reactivity trend would, however, be consistent with increased importance of H-abstraction from the C-H bond or adduct formation. The negative temperature dependence seen for the very fast $(CH_3)_3N$ + O reaction suggests a reaction mechanism involving adduct formation. In this case, direct electrophilic attack at the N-center would yield an excited N-oxime adduct. This can either undergo collisional stabilization or fragmentation to products, or in the case of 1^o and 2^o amine reactions, the initial N-oxime may first rearrange to another excited adduct, a hydroxylamine, which then either collisionally stabilizes or decomposes to final products. To our knowledge, absolute OH or other possible product yield measurements have not been performed for these amine reactions either. Such studies would be very valuable for discerning which reaction path(s) are important in the O-atom oxidation of amines. Hence, by analogy, N-oxime type adduct formation in O + di-amine reactions should upon (rearrangement and) N-N bond cleavage also either lead to a hydroxylamine product plus NH, or NH_2 or HNO and their corresponding co-fragments. To

date, no direct product studies on these species have been carried out. We plan to carryout LIF measurements of these radical fragments in the near future to ascertain their phenomenological branching fractions.[35] Also, future OH and OD product yield measurements in O-atom reactions with N-deuterated hydrazines ($(CH_3)_2NND_2$ and CH_3NDND_2) or with their methyl-deuterated analogues should provide valuable information on the relative importance of removal of the hydrogen from the methyl functionality compared to that from the N-center.

Even though an Arrhenius fit to k_1 and k_2 for the entire temperature range of 232 to 644 K is possible, the data in Figure 3 for T > 500 K clearly shows an onset of upward curvature in the temperature dependence of k_i. In this regime, either the di-amine pyrolytic products are affecting our rate measurements or the importance of another reaction (possibly direct H-abstraction) is increasing. Future higher temperature rate coefficient and OH yield measurements would be of interest for confirming this observation.

Thermospheric Plume Chemistry. From our present data, we calculate k_2 to be ~ 2 x 10-11 cm^3 $molec^{-1}$ s^{-1} for a typical low earth orbit (LEO) thermospheric temperature of around ~ 880 K. Assumption of a nominal number density of ~ 1 x 10^9 molec cm^{-3} for the ambient O-atoms results in an oxidation lifetime of ~ 50 seconds for the CH_3NHNH_2 fuel fragments in the Space Shuttle thruster plume. The oxidation lifetime of the fuel fragments might be much shorter than this for two reasons. Firstly, the thermal rate coefficient at 880 K could be much higher than that extrapolated from Figure 3, and secondly, the hyperthermal oxygen atoms, O*, in the thermosphere could be reacting with the fuel much more vigorously than the thermal atoms which we have measured here to proceed at ~ $1/10^{th}$ the gas kinetic rate. Depending on the

direction of the thruster velocity (~ 3.5 km s^{-1}) relative to the Shuttle's orbital velocity (~ 7.8 km s^{-1}), the di-amine molecules can encounter O* travelling with relative velocities in the range from 4.3 to 11.3 km s^{-1}, which corresponds to collision interaction energies in the range 1.1-7.9 eV. These energetic encounters could have higher overall reaction cross-sections and proceed via several different modes of attack. Perhaps direct abstraction rather than addition/elimination could be the predominant reaction mechanism in the hyperthermal regime. This would lead to entirely different kinds of product branching patterns/state distributions, and therefore ir and (possibly uv) chemiluminescence, than that observed in the room temperature bulb experiments which are characterized by Boltzmann energy distributions. Alternatively, high-energy barrier and/or endothermic channels, and pathways that involve complex geometrical rearrangements with electronic excitement could become more accessible. For the latter type, Orient and co-workers,[36] in their crossed-molecular beam apparatus, have seen evidence for the direct formation of electronically excited radical fragments when very fast, ~ 20 eV, in the laboratory frame (LAB), O* encounters the di-amine molecule. NH(A) emission was seen for all three di-amine reactions under *single-collision* conditions, while CH(A) and CN(B) emissions were seen only for the CH_3NHNH_2 reaction. In an earlier work, they had shown that the threshold for NH(A) production was at ~ 7.0 eV, LAB, in the case of the hydrazine reaction.[37] This suggests $N_2H_4 + O^* \rightarrow NH(A) + NH_2OH$ is the most likely reaction channel for the observed emission since it has a lower thermodynamic threshold of ~ 3.53 eV, in the center-of-mass frame (CM), compared to other possible channels; $\rightarrow NH(A) + H_2O + NH$ and $\rightarrow NH(A) + NH_2 + OH$, which have CM thresholds of ~ 5.32 and ~ 6.28 eV, respectively. The corresponding minimum O* beam energy needed would be ~ 5.29, ~ 7.98 and ~ 9.41 eV, LAB, respectively. Their measured threshold suggests a considerable reaction barrier for excited-state product formation.

No measured reaction threshold energies are available for the O* + alkylated di-amine reactions. However, these should have reaction barriers at least equal to their thermodynamic lower limits. Thus for O* + CH_3NHNH_2, the corresponding product channels; $\rightarrow$ NH(A) + CH_3NHOH, $\rightarrow$ NH(A) + H_2O + CH_3N and $\rightarrow$ NH(A) + CH_3NH + OH would have CM thresholds of $\geq$ 3.41, $\geq$ 2.81 and $\geq$ 6.22 eV, respectively. For the Space Shuttle plume, this means that the reactions would turn on at relative velocities of ~ 7.44, ~ 6.76 and ~ 8.66 km s^{-1}, respectively. Indeed, the NH(A) plume-radiation intensity is observed to show a strong angular dependence on the Shuttle's orbital velocity vector relative to its thrust vector, with an observed cut-off somewhere in between 30° and 90° (zero and 180°, respectively being wake and head-on ram firings). In their numerical simulations, Viereck and co-worker,[10] did not consider direct NH(A) formation from the raw fuel, but rather from similar O* reactions with its pyrolytic product, CH_2NH ($\rightarrow$ NH(A) + H_2CO or $\rightarrow$ NH(A) + H_2 + CO) and combustion products, HNC ($\rightarrow$ NH(A) + CO) and HNCO ($\rightarrow$ NH(A) + CO_2). They ruled out the HNC reaction, since in the plume the HCN isomer should be the favored species, and its reaction with O* is known to produce strong CN(B$\rightarrow$X) emissions in the laboratory.[38] The plume-radiation at 380 nm due to CN(B$\rightarrow$X) was much weaker than that at 336 nm due to NH(A$\rightarrow$X), implying a very low absolute [HNC] relative to that of the NH(A) precursor. The HNCO reaction with its thermodynamic threshold of ~ 2.02 eV, CM, would imply an onset for NH(A) emission at relative collision velocity in LEO of ~ 5.78 km s^{-1}, while the higher ~ 2.49 and ~ 2.47 eV, CM, thermodynamic thresholds for the CH_2NH reactions would imply onset at ~ 6.80 and ~ 6.78 km s^{-1}, respectively. Consequently, the higher angle(s) (between the orbital and thrust vectors) predicted by the latter reactions for the emission onset gave better agreement with the observations, and therefore,

HNCO was also ruled out. Note that the O* + CH_3NHNH_2 reaction(s), from above, would also have similar high angle onset(s). It is not clear whether or not Viereck and co-worker explicitly were able to rule out this direct path for NH(A) in their *spacecraft/orbiter contamination representation accounting for transiently emitted species* (SOCRATES) simulations, rather they stipulated that a precursor (CH_2NH) mole fraction of ~ 3 x 10^{-5} and inclusion of its O* reaction in the code gave a reasonable reproduction of many of the observed NH(A) plume-radiation features, including the variation of its intensity with the ram angle. To our knowledge, neither the O* + $CH_2NH \rightarrow NH(A) + H_2CO$ (or $\rightarrow NH(A) + H_2 + CO$), nor the HNC + O* $\rightarrow$ NH(A) + CO, or the HNCO + O* $\rightarrow$ NH(A) + CO_2 reactions have been studied in the laboratory. Also, the relative CH_2NH and CH_3NHNH_2 concentrations in di-amine thermospheric plumes have not been directly measured accurately enough[40] to say conclusively what is the dominant source of the NH(A) radiation. The source region of the hypothesized CH_2NH species could be the exhaust exit plane or in-situ production in the plume. If latter is the case, then since the fuel's pyrolytic lifetime[41] is expected to be as short as ~ $1/50^{th}$ of a second in the vicinity of the spacecraft, the choice of CH_2NH over CH_3NHNH_2 reaction as the principle NH(A) source would seem to be very logical. However, pyrolysis of the fuel in the plume would initially give CH_3NH and NH_2 as the main products. Therefore, the relative importance of CH_3NH disproportionation reaction to yield CH_2NH plus CH_3NH_2 compared to its hyperthermal oxidative loss first needs to be understood properly for LEO conditions before the results of SOCRATES or any other numerical simulations can be correctly interpreted in terms of what dominant processes give rise to the measured NH(A) optical environment of the di-amine fueled thermospheric plume.

The (far-field) spectrum of the plume from the Space Shuttle's primary RCS (Figure 3 of Ref. 10) also shows prominent OH(A→X) emissions. We are not aware of any detailed analysis for its emission as a function of the spacecraft's altitude or its ram angle dependence. The following can be said about the possible nature of its source. If the intensity varies with altitude in a manner that is directly proportional to the O-atom density profile, then the reaction is with a precursor which itself was not formed by a prior thermospheric O-atom oxidative step, since the latter route would give a variation in intensity that would be quadratic in dependence with the O-atom density. Either combustion effluent(s), for example H_2O,[42] or raw fuel reaction(s) with the O-atoms could produce this radiation. The former reaction with a thermodynamic threshold of ~ 4.79 eV, CM, has been hypothesized to be important since H_2O is the most abundant hydrogenous species in exhaust plumes. Recent OH(A→X) emission data[43,44] of the Progress-M Spacecraft have been analyzed, with some success,[44,45] using the $H_2O + O^* \rightarrow OH(X) + OH(A)$ source chemistry. However, the energetically less demanding $CH_3NHNH_2 + O^* \rightarrow OH(A) + CH_3N_2H_2$ reaction, with a threshold of ~ 2.82 eV, CM, may also be important at $\geq$ ~ 6.78 km s^{-1} LEO collisional velocity in the case of the Space Shuttle. Thus one should see an angular onset of OH emission very similar in nature to that observed for NH(A). In principle, the mechanism for this hyperthermal reaction might just be ('direct') H-abstraction with electronic excitation in the OH product. The extent to which translational excitation in the reactant couples to higher electronic degrees of freedom in the product, and its reaction mechanism and dynamics are amongst the least understood molecular processes in the gas phase. However, the related hyperthermal ions, O^{+*}, are known to react with di-amines to produce uv-

visible emissions under laboratory conditions. [47] The proposed mechanism for the emission involves two steps: an initial charge transfer (possibly a dissociative) process to give the di-amine$^+$ (or a daughter$^+$) ion, followed by a dissociative recombination step of the cation(s) with the residual plasma electrons to give electronically excited fragment(s). Such processes in LEO are expected to be of minor importance since the ion density (of which ~ 98% is due to O^{+*}) is typically ~ 10^4 times less than the ambient O* density. Since Orient and co-workers[36] did not report uv measurements below ~ 325 nm, we plan to search for OH(A→X) emissions in ≥ 5 eV-O*-atom interactions with N_2H_4 and CH_3NHNH_2.[35]

To our knowledge, *ab-initio* molecular orbital theory computational study on the O + N_2H_4 reaction has not been performed. It should be interesting to see if an overall energetic profile typical of an addition-elimination mechanism is calculated at thermal energies, and what the predictions are for the transition states and reaction intermediates. Also, of interest would be RRKM/TS-theory predictions for the absolute value for the rate coefficient and the product branching fractions and their temperature and pressure dependencies, and QCT simulations on the derived PES to ascertain the nature of product state distributions as a function of the collision energy.

CONCLUSIONS

For the first time, the O-atom rate coefficients for gas phase reactions with $(CH_3)_2NNH_2$ and CH_3NHNH_2 have been measured in the range 232-644 K and in He pressure of 2.0 torr, and

are shown to have weak (negative) temperature dependencies as was the case with the $O + N_2H_4$ reaction. The lack of any pressure dependence in the latter reaction, and the low OH yields measured in all ~~these~~ three reactions suggest a complex reaction mechanism involving the formation of an initial adduct which then rapidly dissociated into a variety of products. Previous studies have shown H_2O plus the di-imide co-fragment to be the dominant products in the reaction(s). Future experimental product(s) state distribution and/or alignment measurements (for instance for the OH product[35]) should provide valuable dynamical/mechanistic information about the predominant forces and torques that are exerted as the transient $\{ON_2H_4\}^*$ species unfolds into products.

ACKNOWLEDGMENT

Funding for this work was provided by the Air Force Office of Scientific Research under Contract # F04611-99-C-0025 with the Air Force Research Laboratory, Edwards AFB, CA 93524.

REFERENCES

(1) Sutton, G. P. *Rocket Propulsion Elements. An Introduction to the Engineering of Rockets*; Wiley: New York, 1992.

(2) Trinks, H.; Hoffman, R. J. *Experimental Investigations of Bipropellant Exhaust Plume Flowfield, Heating, and Contamination and Comparison With CONTAM Computer Model Predictions*, in *Spacecraft Contamination: Sources and Preventions*; Roux, J. A.;

McMay, T. D. Eds.; Progress in Astronautics and Aeronautics, AIAA: New York, NY, 1984; Vol. 91, p. 261.

(3) Viereck, R. A.; Bernstien, L. S.; Mende, S. B.; Murad, E.; Swenson, G. H.; Pike, C. P. *J. Spacecraft Rockets* **1993**, 30, 724.

(4) Viereck, R. A.; Murad, E.; Pike, C. P.; Mende, S. B.; Swenson, G. R.; Elgin, J. B.; Bernstein, L. S.; Lucid, S. *J. Geophys. Res.* **1995**, A100, 5819.

(5) Koch, D. G.; Fazio, G. G.; Hoffmann, W.; Melnick, G.; Rieke, G.; Simpson, J.; Witteborn, F.; Young, E. *Adv. Space Res.* **1987**, 7, 211.

(6) Dean, D. A.; Huppi, E. R.; Smith, D. R.; Nadile, R. M.; Zhou, D. M. *Geophys. Res. Lett.* **1994**, 21, 609.

(7) Zhou, D. K.; Pendleton, W. R. Jr.; Bingham, G. E.; Thompson, D. C.; Raitt, W. J.; Nadile, R. M. *J. Geophys. Res.* **1994**, A99, 19585.

(8) Bernstein, L. S.; Elgin, J. B.; Pike, C. P.; Knecht, D. J.; Murad, E.; Zehnpfennig, T. F.; Galica, G. E.; Stair, A. T. Jr. *J. Geophys. Res.* **1996**, A101, 383.

(9) Broadfoot, A. L.; Anderson, E.; Sherard, P.; Knecht, D. J.; Viereck, R.A.; Pike, C. P.; Murad, E.; Elgin, J. E.; Bernstein, L. S.; Kofsky, I. L.; Rall, D. L. A.; Blaha, J.; Culbertson, F. L. *J. Geophys. Res.* **1992**, A97, 19501.

(10) Viereck, R. A.; Murad, E.; Knecht, D. J.; Pike, C. P. *J. Geophys. Res.* **1996**, A101, 5371.

(11) Lang, V. I. *J. Phys. Chem.* **1992**, 96, 3047.

(12) Shane, E. C.; Brennen, W. *J. Chem. Phys.* **1971**, 55, 1479.

(13) Gehring, von M.; Hoyermann, K.; Wagner, H. Gg.; Wolfrum, J. *Ber. Bunsenges Phys. Chem.* **1969**, 73, 956 and Gehring, M.; Hoyermann, K.; Schacke, H.; Wolfrum, J. *Symp. (Int.) Combust. Proc.* **1972**, 14, 99.

(14) Vaghjiani, G. L. *J. Chem. Phys.* **1996**, 104, 5479.

(15) Foner, S. N.; Hudson, R. L. *J. Chem. Phys.* **1968**, 49, 3724 and **1970**, 53, 4377.

(16) Vaghjiani, G. L. *J. Phys. Chem. A* **1997**, 101, 4167.

(17) Vaghjiani, G. L. *J. Chem. Phys.* **1993**, 98, 2123.

(18) Howard, C. J. *J. Phys. Chem.* **1979**, 83, 3, and references therein.

(19) Raiche, G. A.; Jeffries, J. B.; Rensberger, K. J.; Crosley, D. R. *J. Chem. Phys.* **1990**, 92, 7258, and Dodd, J. A.; Lipson, S. T.; Blumberg, W. A. M. *J. Chem. Phys.* **1991**, 95, 5752.

(20) Vaghjiani, G. L.; Ravishankara, A. R. *J. Phys. Chem.* **1989**, 93, 1948.

(21) Zelikoff, M.; Watanabe, K.; Inn, E. C. Y. *J. Chem. Phys.* **1953**, 21, 1643.

(22) Cantrell, C. A.; Zimmer, A.; Tyndall, G. S. *Geophys. Res. Lett.* **1997**, 24, 2195, and **1997**, 24, 2687.

(23) Barth, C. A.; Suess, H. E. Z. *Physik.* **1960**, 158, 85, and Stief, L. J.; Payne, W. A.; Klemm, R. B. *J. Chem. Phys.* **1975**, 62, 4000.

(24) Turnipseed, A. A.; Vaghjiani, G. L.; Gierczak, T.; Thompson, J. E.; Ravishankara, A. R. *J. Chem. Phys.* **1991**, 95, 3244.

(25) DeMore, W. B.; Sander, S. P.; Howard, C. J.; Ravishankara, A. R.; Golden, D. M.; Kolb, C. E.; Hampton, R. F.; Kurylo, M. J.; Molina, M. J. *Chemical Kinetics and Photochemical Data for Use in Stratospheric Modeling;* Evaluation No. 12, JPL Publication No. 97-4 (Jet Propulsion Laboratory, Pasadena, CA 1997), and references therein.

(26) Ogawa, M. *J. Chem. Phys.* **1971**, 54, 2550.

(27) Inn, E. C. Y.; Heimerl, J. M. *J. Atmos. Sci.* **1971**, 28, 838, and Kosh, M.; Yoshimura, M.; Matsui, H. *Chem. Phys. Lett.* **1991**, 176, 519.

(28) Bailey, E. A.; Heard, D. E.; Paul, P. H.; Pilling, M. J. *J. Chem. Soc., Faraday Trans.* **1997**, 93, 2915, Wysong, I. J.; Jeffries, J. B. Crosley, D. R. *J. Chem. Phys.* **1990**, 92, 5218, Copeland, R. A.; Crosley, D. R. *J. Chem. Phys.* **1986**, 84, 3099, and Copeland, R. A.; Dyer, M. J.; Crosley, D. R. *J. Chem. Phys.* **1985**, 82, 4022.

(29) German, K. R. *J. Chem. Phys.* **1975**, 63, 6262.

(30) Tuazon, E. C.; Carter, W. P. L.; Winer, A. M.; Pitts, J. N. Jr. *Environ. Sci. Technol.* **1981**, 15, 823.

(31) Vaghjiani, G. L. *Int. J. Chem. Kinet.* **2000**, submitted.

(32) Foner, S. N.; Hudson, R. L. *Advan. Chem. Ser.* **1962**, 36, 34.

(33) Gejo, T.; Felder, P.; Huber, J. R. *Chem. Phys.* **1994**, 195, 423, and references therein.

(34) Atkinson, R.; Pitts, J. N. Jr. *J. Chem. Phys.* **1978**, 68, 911.

(35) Vaghjiani, G. L. work in progress.

(36) Orient, O. J.; Chutjian, A.; Murad, E. *J. Chem. Phys.* **1994**, 101, 8297.

(37) Orient, O. J.; Chutjian, A.; Martus, K. E.; Murad, E. *J. Chem. Phys.* **1992**, 97, 4111.

(38) Orient, O. J.; Chutjian, A.; Martus, K. E.; Murad, E. *Phys. Rev. A* **1993**, 48, 427.

(40) Wulf, E.; Zahn, von U. *J. Geophys. Res.* **1986**, A91, 3270.

(41) Eberstein, I. J.; Glassman, I. *Symp. (Int.) Combust. Proc.* **1965**, 10, 365.

(42) Orient, O. J.; Chutjian A.; Murad, E. *Phys. Rev. Lett.* **1990**, 65, 2359.

(43) Karabadzhak, G. F.; Plastinin, Y.; Khmelinin, B.; Teslenko, V.; Shvets, N.; Drakes, J. A.; Swann, D. G.; McGregor, W. K. in *AIAA 36th Aerospace Science Meeting & Exhibition;* AIAA-98-0288, Reno, NV, January 1998.

(44) Drakes, J. A.; Swann, D. G.; Karabadzhak, G. F.; Plastinin, Y. in *AIAA 37th Aerospace Science Meeting & Exhibition;* AIAA-99-0975, Reno, NV, January 1999.

(45) Karabadzhak, G. F.; Plastinin, Y.; Szhenov, E.; Afanasjev, A.; Drakes, J. A.; McGregor, W. K.; Bradley, D.; Teslenko, V.; Shvets, N.; Volkov, O.; Kukushkin, V.; Gimelshein, S.; Levin, D. A. in *AIAA 38th Aerospace Science Meeting & Exhibition;* AIAA-00-0105, Reno, NV, January 2000.

(47) Gardner, J. A.; Dressler, R. A.; Salter, R. H. *J. Phys. Chem.* **1994**, 98, 11636.

FIGURE CAPTIONS

Figure 1 Measured O-atom resonance fluorescence signal, as a function of flow-tube reaction time, t in different $(CH_3)_2NNH_2$ concentrations; = zero (open circles), = 0.587 x 10^{13} (solid squares), = 0.643 x 10^{13} (open squares), and = 0.957 x 10^{13} molec cm^{-3} (solid triangles), at 371 K and in 1.96 torr He. The OH is produced in the side-arm port.

Figure 2 Plot of pseudo-first-order decay coefficients, $k_{net} = (k'_1 + k'_{w,in})$ versus the $[(CH_3)_2NNH_2]$ of Figure 1. Because the upward correction, of k_{net} for axial diffusion, $k_{corr} = k_{net}(1 + k_{net}\mathcal{D}/v^2)$, where $\mathcal{D}$, in units of $cm^2\ s^{-1}$, is the diffusion coefficient of O-atoms in He is expected to be < 5%, Ref. 18, the flow-tube data was not corrected for this since the other overall errors in the experiment are calculated to be ~ ± 18%, Ref. 14. The absolute second-order rate coefficient, k_1 is determined to be (2.05 ± 0.36) x 10^{-11} cm^3 $molec^{-1}$ s^{-1} at 371 K.

Figure 3 The Arrhenius temperature dependencies of the absolute second-order rate coefficients; k_1 and k_2 for O-atom reactions with $(CH_3)_2NNH_2$ (open triangles) and CH_3NHNH_2 (open circles), respectively. The 1-σ error bars represent, on average, an overall uncertainty of ~ ± 18% in the rate coefficient values. Previous room temperature results for k_1 (solid triangle) and k_2 (solid circle) from Ref. 11 are also shown.

Figure 4 (a) OH appearance profile in O + CH_3NHNH_2 reaction studied in the flow-tube apparatus. (b) OH appearance profile in O + N_2H_4 reaction during 193-nm photolysis of N_2O (2.1 x 10^{15}) in N_2 (6.9 x 10^{17}) and CO_2 (8.1 x 10^{16} molec cm^{-3}). The laser fluence was ~ 1.5

mJ/cm^2/pulse and N_2H_4 concentration was 1.10 x 10^{13} molec cm^{-3}. The characteristic coefficients of appearance and decay in the signals yield values for $k'_{i,OH}$ and k'_i, respectively. Where k'_i and $k'_{i,OH}$, are respectively, the first-order rate coefficients for O-atom and OH radical reactions in the system.

Figure 5 Second-order plots for O + CH_3NHNH_2 flow-tube reaction at 298 K and in 2.0 torr He pressure: (a) decay coefficients, k'_2 directly determined by O-atom detection (open triangles) and by fitting observed OH product profile of Figure 4 (a) to a bi-exponential kinetic expression (solid triangles). (b) the corresponding appearance coefficients, $k'_{2,OH}$ in the bi-exponential fit. (c) phenomenological OH branching coefficient (RHS of Equation (II)) determined by comparison of growth in the OH signal relative to decay of the O-atom signal, see text.

'gure 1

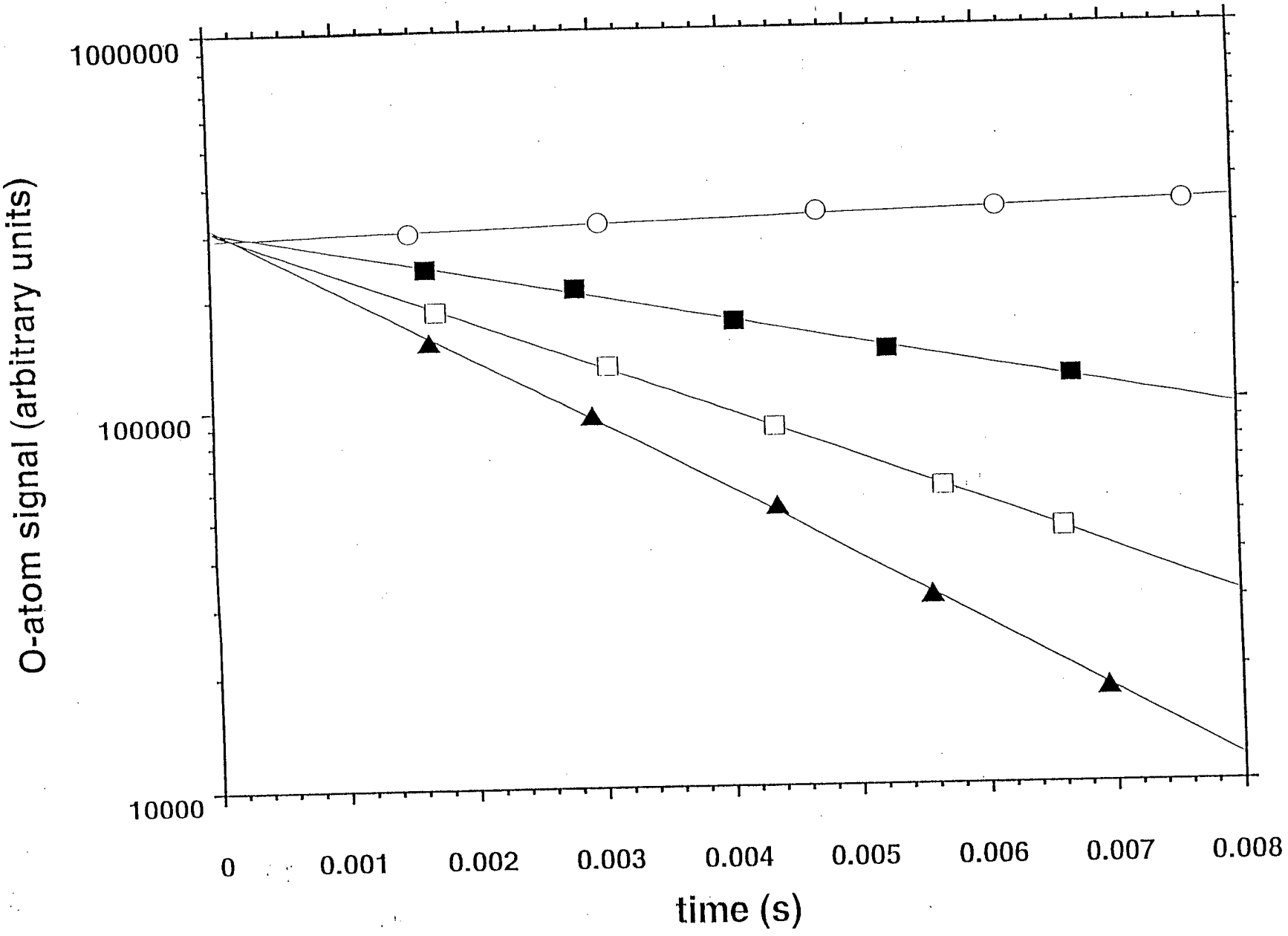
1000000
100000
10000
O-atom signal (arbitrary units)
0
0.001
0.002
0.003
0.004
0.005
0.006
0.007
0.008
time (s)

gure 2

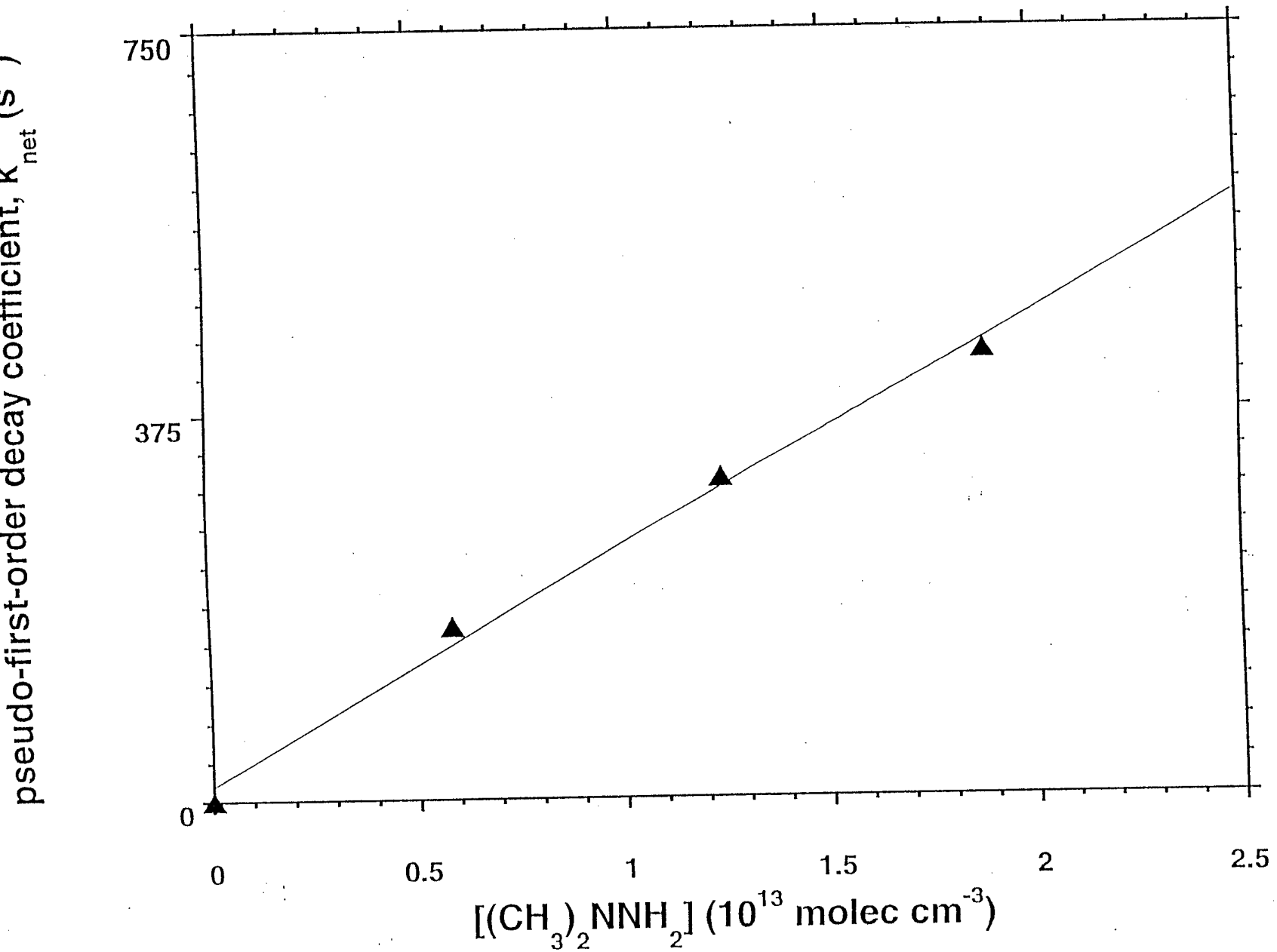
pseudo-first-order decay coefficient, k_{net} (s^{-1})
750
375
0
0
0.5
1
1.5
2
2.5
$[(CH_3)_2NNH_2]$ (10^{13} molec cm^{-3})

gure 3

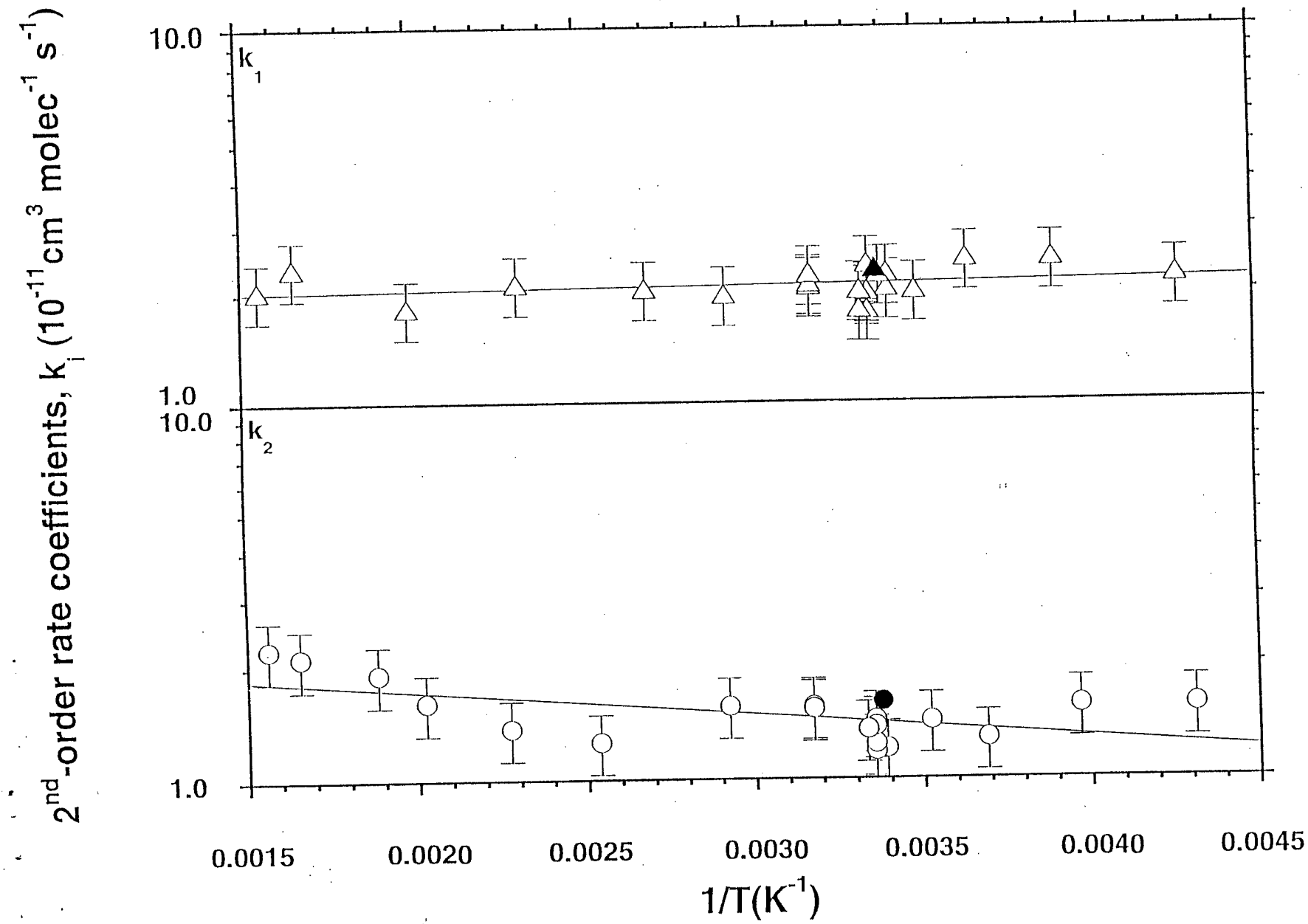
10.0
k1
1.0
10.0
k2
1.0
0.0015
0.0020
0.0025
0.0030
0.0035
0.0040
0.0045
1/T(K-1)
2nd-order rate coefficients, kj (10-11cm3 molec-1 s-1)

Figure 4

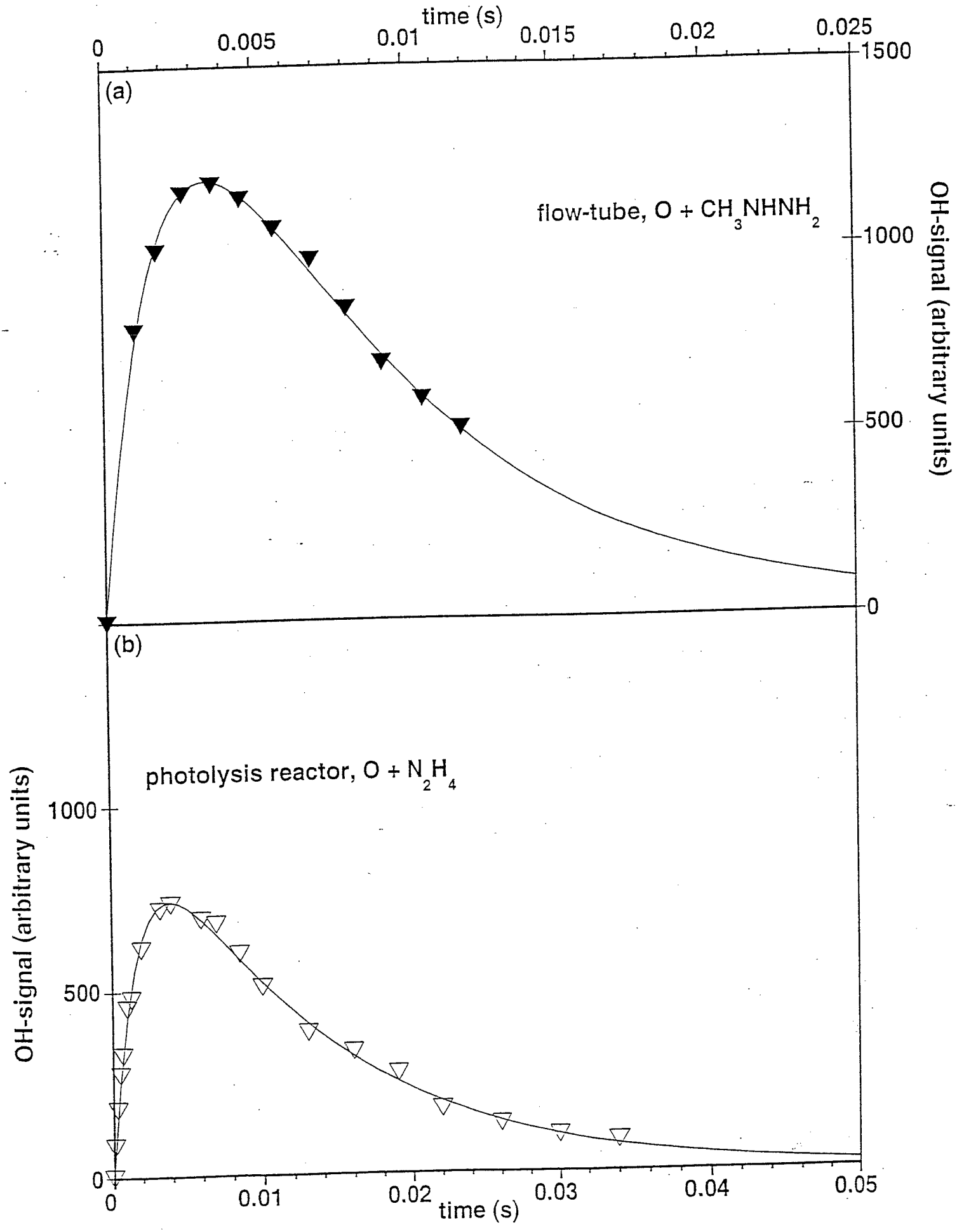
time (s)
0
0.005
0.01
0.015
0.02
0.025
(a)
flow-tube, O + CH3NHNH2
1500
1000
500
0
OH-signal (arbitrary units)
(b)
photolysis reactor, O + N2H4
1000
500
0
OH-signal (arbitrary units)
0
0.01
0.02
0.03
0.04
0.05
time (s)

Figure 5

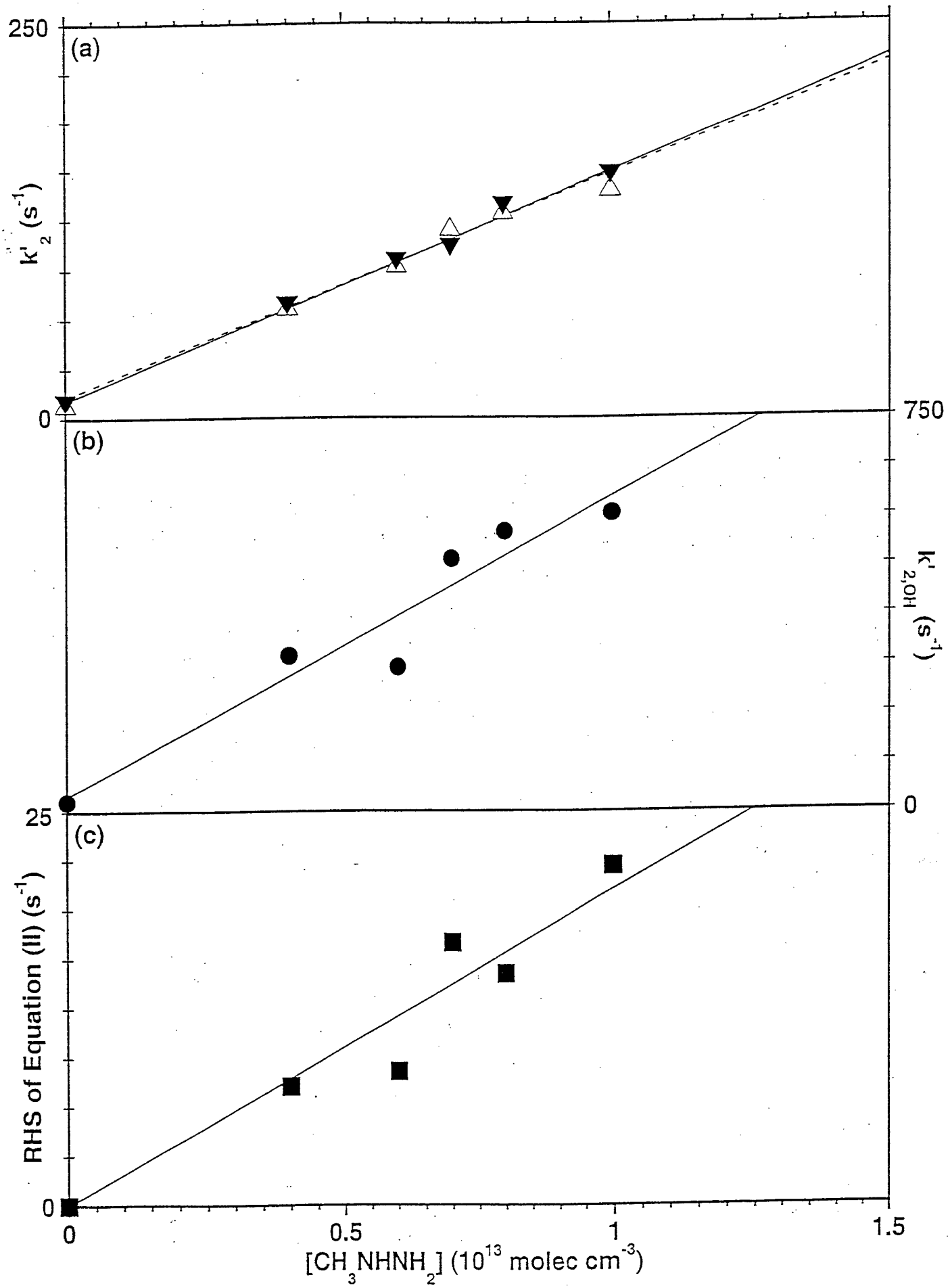
250
(a)
k'_2 (s^{-1})
0
750
(b)
$k'_{2,OH}$ (s^{-1})
25
(c)
RHS of Equation (II) (s^{-1})
0
0
0.5
1
1.5
[CH_3NHNH_2] (10^{13} molec cm^{-3})